Self-assembly of a sulphur-terminated graphene nanoribbon within a single-walled carbon nanotube

A. Chuvilin[1,2], E. Bichoutskaia[3], M. C. Gimenez-Lopez[3], T. W. Chamberlain[3], G. A. Rance[3], N. Kuganathan[3], J. Biskupek[4], U. Kaiser[4] and A. N. Khlobystov[3]*

[1]CIC nanoGUNE Consolider, Tolosa Hiribidea 76, E-20018, Donostia-San Sebastian, Spain, [2]IKERBASQUE, Basque Foundation for Science, 48011 Bilbao, Spain, [3]School of Chemistry, University of Nottingham, University Park, Nottingham NG7 2RD, UK, [4]Central Facility of Electron Microscopy, Group of Electron Microscopy of Materials Science, Ulm University, Albert-Einstein-Allee 11, D-89081 Ulm, Germany. *e-mail: andrei.khlobystov@nottingham.ac.uk.

ABSTRACT

The ability to tune the properties of graphene nanoribbons (GNRs) through modification of the nanoribbon's width and edge structure[1–3] widens the potential applications of graphene in electronic devices[4–6]. Although assembly of GNRs has been recently possible, current methods suffer from limited control of their atomic structure[7–13], or require the careful organization of precursors on atomically flat surfaces under ultra-high vacuum conditions[14]. Here we demonstrate that a GNR can self-assemble from a random mixture of molecular precursors within a single-walled carbon nanotube, which ensures propagation of the nanoribbon in one dimensionand determines its width. The sulphur-terminated dangling bonds of the GNR make these otherwise unstable nanoribbons thermodynamically viable over other forms of carbon. Electron microscopy reveals elliptical distortion of the nanotube, as well as helical twist and screw-like motion of the nanoribbon. These effects suggest novel ways of controlling the properties of these nanomaterials, such as the electronic band gap and the concentration of charge carriers.

Single-walled carbon nanotubes (SWNTs) with typical diameters of 0.7–2.0 nm are ideal containers for medium-sized molecules. Carbon cages of fullerenes, having a particularly strong affinity for the interiors of nanotubes, have been studied within nanotubes more than any other molecular species[15]. Triggered by heat or electron beam (e-beam) radiation, fullerenes undergo chemical transformations in SWNTs. Although the nanotube itself is not involved in the reactions of the guest-molecules, it imposes severe limitations on the structure of the product formed[16]. For example, fullerene epoxide ($C_{60}O$) forms strictly linear polymer chains within a SWNT, whereas the same reaction taking place outside the nanotube leads to the formation of branched, highly convoluted polymers[16]. This clearly illustrates the unique ability of nanotubes to act not only as containers, but also as efficient templates for the synthesis of structures that otherwise would not exist.

Under harsh heating (>800 °C) or e-beam irradiation conditions, more drastic transformations of molecules can also take place inside nanotubes. Fullerenes, for example, break down into small clusters of atoms and transform into a narrow nanotube nestled within the original host-SWNT, producing a SWNT@SWNT system[17]. Once again, the host-nanotube acts as a template that prevents the formation of the thermodynamically most stable form of carbon (namely graphite) by restricting the growth in two dimensions, leading to the formation of a 1D structure (namely the guest-SWNT). In principle, the 1D structure of acarbon nanoribbon is also compatible with the geometry of the host-SWNT, but in practice the growth of GNRs has never been observed in nanotubes. Our calculations of the Gibbs free energy of formation (per atom) δG for various 1D nanostructures clearly indicate that a guest-SWNT is significantly more stable than a GNR of a similar width (Fig. 1 and Supplementary Table S1), despite the fact that the bond lengths and angles of the latter are closer to the ideal geometry of an sp^2-carbon atom. The key reason for the lower stability of GNRs is related to the unsaturated valences of the carbon atoms at the edge of the nanoribbon, which have only two bonds instead of the three that are required for an sp^2-carbon atom. However, interestingly, once the edges of the nanoribbon are terminated with heteroatoms (for exampleH or other non-carbon elements), the resultant edge-terminated GNR becomes thermodynamically more stable than a SWNT (Fig. 1). These simple structural and energetic considerations give an explanation why GNRs cannot be formed from fullerenes and, most importantly, provide a key recipe for the construction of nanoribbons in nanotubes: the growth of stable GNRs requires plenty of carbon—a building element of the GNR itself, as well as some non-carbon elements able to terminate all the edges of the GNR.

The carbon cages of fullerenes possess a rich chemical reactivity that allows the grafting of organic functional groups to the fullerene surface. Thus functionalized fullerenes still retain their exceptional affinity for the interior of the SWNT (refs 18,19), and therefore can be used as shuttles to transport effectively any elements forming the functional group into the nanotube (Fig. 2). The presence of non-carbon elements in the nano-container widens the range of chemical transformations that could take place within thehost-SWNT and offers a mechanism for terminating the edgesof a nanoribbon. To test this hypothesis, we have designed a complex functional group consisting of a pyrrolidine ring linked to a phenyl ester moiety bearing an alkyl chain with a dithiolane group (Fig. 2a). In addition to 80 atoms of carbon forming the fullerene cage, this molecule contains a selection of hetero-elements H, O, N and S—any of which, in principle, is able to terminate the edge of the GNR (the chemical reactivity of Sc atoms does not allow them to terminate the edges of the GNR). Time series of aberration-corrected high resolution transmission electron microscopy (AC-HRTEM) images reveal that the functional groups of these molecules become fragmented by the 80 keV electron beam[20], followed by breakage of the fullerene cages themselves (Supplementary Fig. S1), thus forming a dynamic mixture of several chemical elements within the cavity of the host-nanotube.

Under prolonged exposure to the e-beam, molecules containing no elements that could saturate the valences of sp^2-carbon (for example C_{60}, $M@C_{82}$) invariably convert into a guest-SWNT

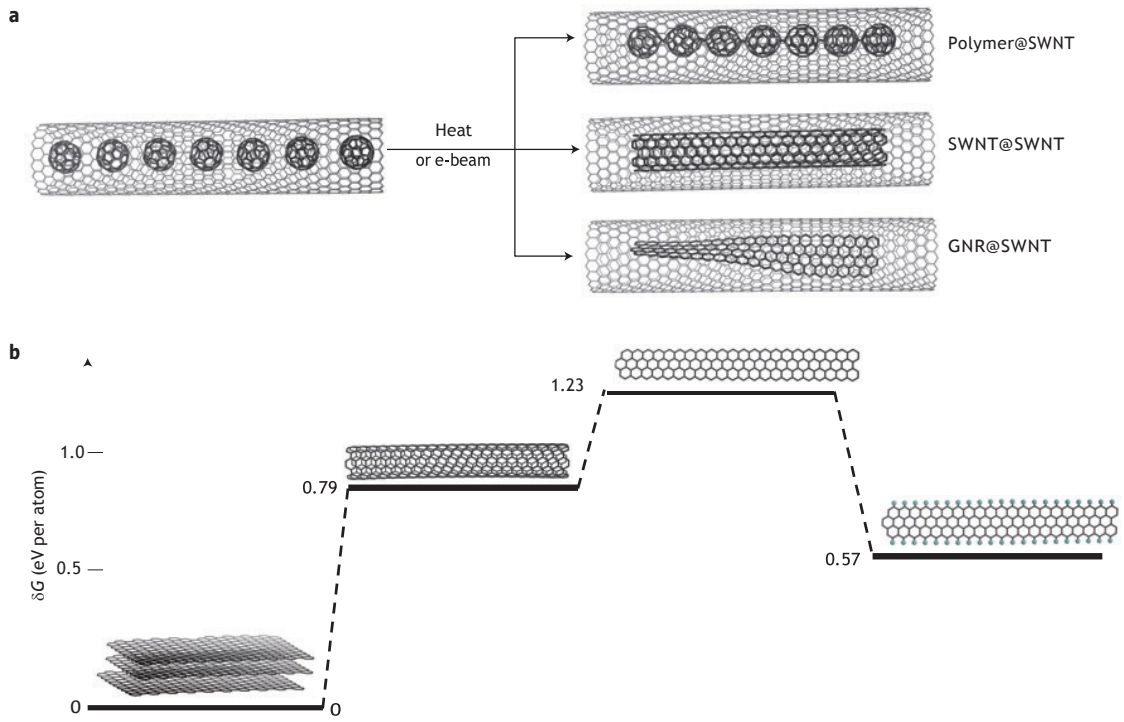

Figure 1 |Guest molecules encapsulated within a carbon nanotube can be transformed into a 1D structure under the influence of heat or an electron beam. a, The host-SWNT acts as a template that allows the growth only in one direction. Depending on the conditions, the molecules of fullerene can either be transformed into a polymer (polymer@SWNT) or into a narrow internal nanotube (SWNT@SWNT); although the formation of a nanoribbon within a SWNT is also possible in theory, GNR@SWNT have never been previously observed. **b**, Comparison of the Gibbs free energy (δG) for different carbon nanostructures clearly shows that a narrow SWNT (0.79 eV per atom) is more thermodynamically stable than a nanoribbon (1.23 eV per atom). The decrease in stability predicted for a GNR is due to the dangling bonds along its edges. Once the edges are terminated with H, S or other non-carbon elements (that is, all dangling bonds are saturated), the terminated nanoribbon becomes more stable (0.57 eV per atom) than a SWNT.

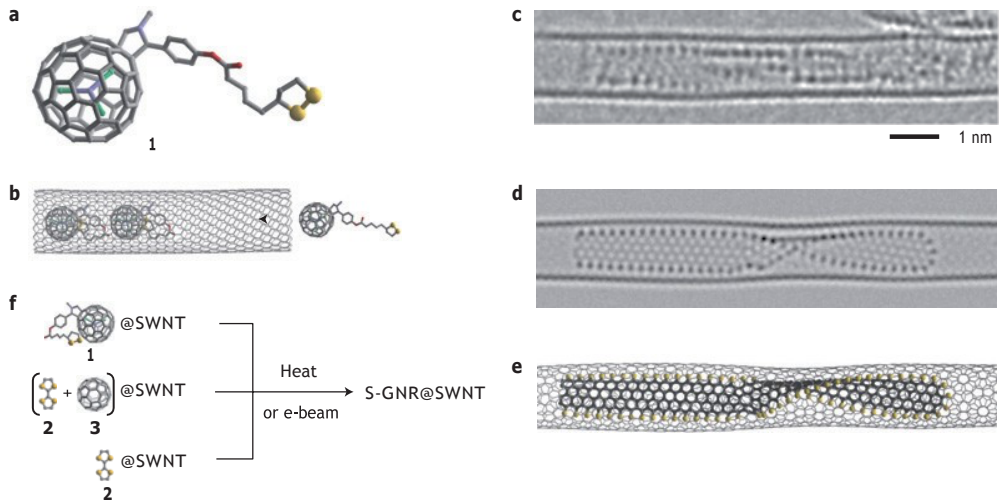

Figure 2 |Carbon nanotubes serve as containers and nanoreactors for molecules. Functionalized fullerenes **1** (**a**) bearing an organic group with sulphur atoms on their surface are spontaneously and irreversibly encapsulated into a SWNT (**b**) owing to the strong van der Waals interactions between the fullerene cage and the interior of the host-nanotube. Under prolonged exposure to the e-beam, the functional groups and the fullerene cages decompose and re-assemble into a nanoribbon inside a (14, 5)-SWNT (**c**). Sulphur atoms terminating the edges of the nanoribbon appear as chains of dark atoms (**c**, an experimental AC-HRTEM image, **e**, a model of S-GNR@SWNT and **d**, an image simulated from the model). Sulphur-terminated nanoribbons can also be formed from other sulphur-containing organic molecules, such as TTF **2** or a mixture of TTF **2** and C_{60} **3** inserted in nanotubes (**f**) at high temperature (1,000 °C) or under e-beam radiation. (In the structural diagrams atoms of sulphur, oxygen, nitrogen and carbon are coloured in yellow, red, blue and grey respectively; atoms of hydrogen in the structural diagram of **1** are omitted for clarity.)

(refs 21,22). However, the functionalized fullerene under similar conditions forms a completely different structure, consisting of two chains of dark atoms running parallel to each other (Fig. 2c). A close inspection of the space between the chains reveals three rows of fused hexagonal rings, equivalent to those in graphene (Fig. 2c). As only sulphur has an atomic number high enough

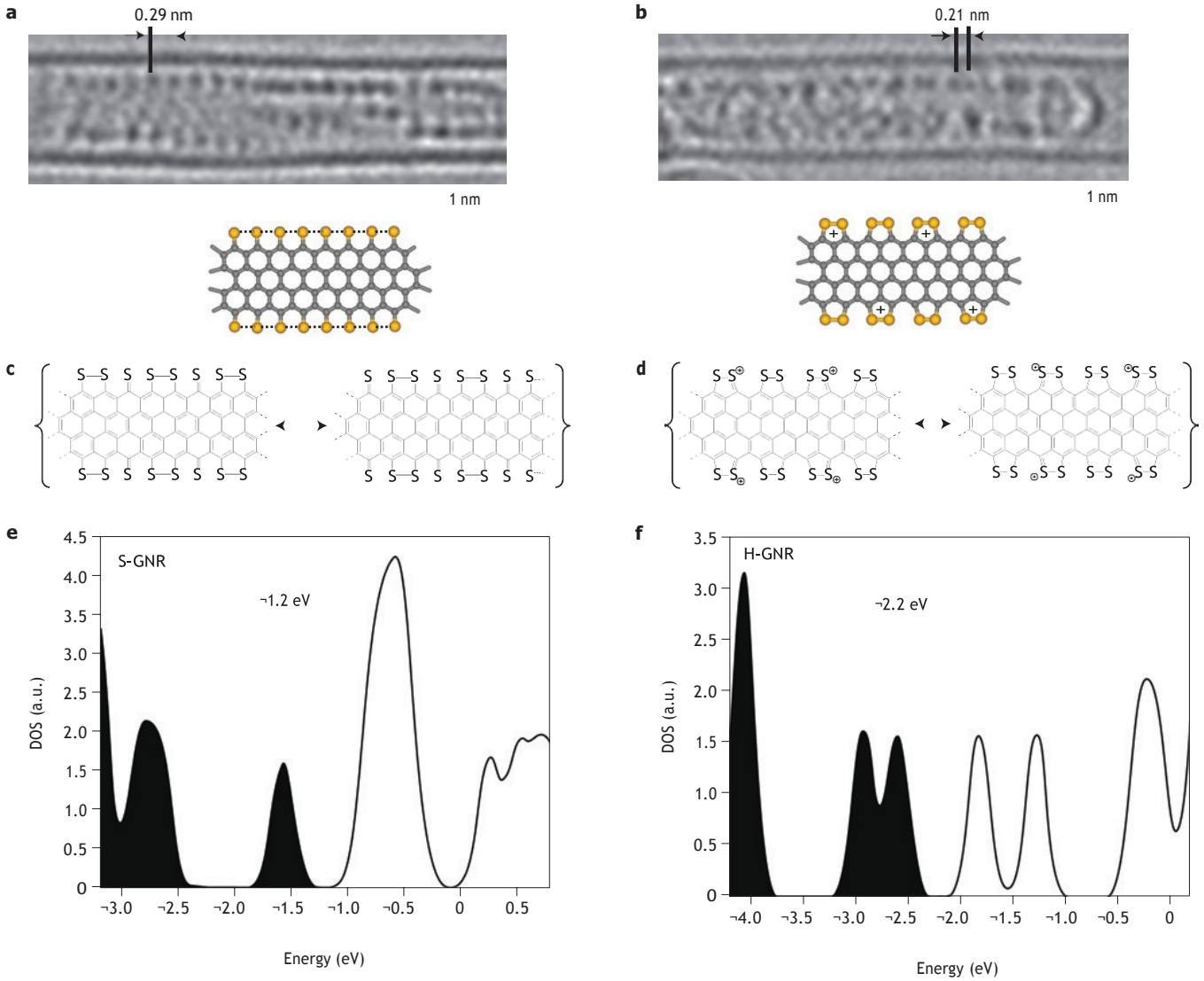

Figure 3 | Structure and properties of sulphur-terminated nanoribbon. At the beginning of the exposure to the e-beam, the sulphur atoms at the edge of the nanoribbon are equidistantly spaced by 0.29 nm (**a**), indicating weak bonding between the neighbouring atoms (the bond order of the S-S bond is less than one; **c**—some resonance forms of the S-GNR). Extensive irradiation with the e-beam removes some of the valence electrons and 'oxidizes' the S-GNR (**b**) causing formation of dithiolium pentagonal rings where the S-S bond has an order of one (**d**—some resonance forms of $[\text{S-GNR}]^{n+}$). As a result, the sulphur atoms are observed in pairs. The density of states calculated for S-GNR (**e**) and H-GNR (**f**) illustrate that termination of the GNR with sulphur atoms maintains the semiconducting character of the nanoribbon but substantially shifts its Fermi level (indicated by a dashed line), thus making the nanoribbon more electron donating. States populated with electrons and empty states are shown as black and white bands respectively.

(*Z* 16) to account for the observed dark atoms (the single-atom contrast of N and O will be much lower and indistinguishable from that of C)[23], these observations are consistent with a zigzag nanoribbon with edges that are terminated by sulphur atoms (S-GNR, Figs 2e, 3a, Supplementary Video S1). In the presenceof a plentiful supply of other elements (H, N, O) terminationwith sulphur is fairly unexpected. However, considering that the nanoribbon is formed under a continuous bombardment of the e-beam, sulphur atoms are least likely to be removed owing to the collisions with electrons, as the energy transferred from the e-beam to the atom is inversely proportional to its atomic number[24]. Therefore, lighter elements (N, O and particularly H) would be stripped away by the e-beam very quickly, making them less suitable for the termination of GNRs.

The selective affinity of the nanoribbon for sulphur atoms was confirmed by the observation that GNRs can be readily formed from a mixture of C_{60} and tetrathiafulvalene (TTF, a sulphur rich molecule with the formula $C_6H_4S_4$) or even from tetrathiafulvalene itself inserted in SWNT (Fig. 2f and Supplementary Figs S2–S4 and Video S2). The observed nanoribbons were up to 20 nm inlength, and energy dispersive X-ray (EDX) spectroscopy confirmed the nature of the atoms terminating their edges as sulphur (Supplementary Fig. S3). Most importantly, the formation of S-GNR was shown to be triggered by heat as well as by e-beam radiation, thus giving a route for the mass production of these nanostructures. Raman spectroscopy (recorded using a green laser at λ_{ex} =538 nm) shows that the vibrational bands of TTF@SWNTat 1,420 cm^{-1} and 490 cm^{-1}, corresponding to a C=C stretch and pentagonal ring bend respectively, after heating at 1,000 °C become replaced by a C=S bond stretch at ~1,200 cm^{-1} of the nanoribbon edge (the vibrations of the carbon–carbon bonds of the S-GNR are obscured by the Raman bands of the SWNT; Supplementary Fig. S5). These examples illustrate that the formation of GNRsis a spontaneous self-assembly process that can take place from a random mixture of atoms (as long as it contains C and S),regardless of the actual structure of the molecular precursors and

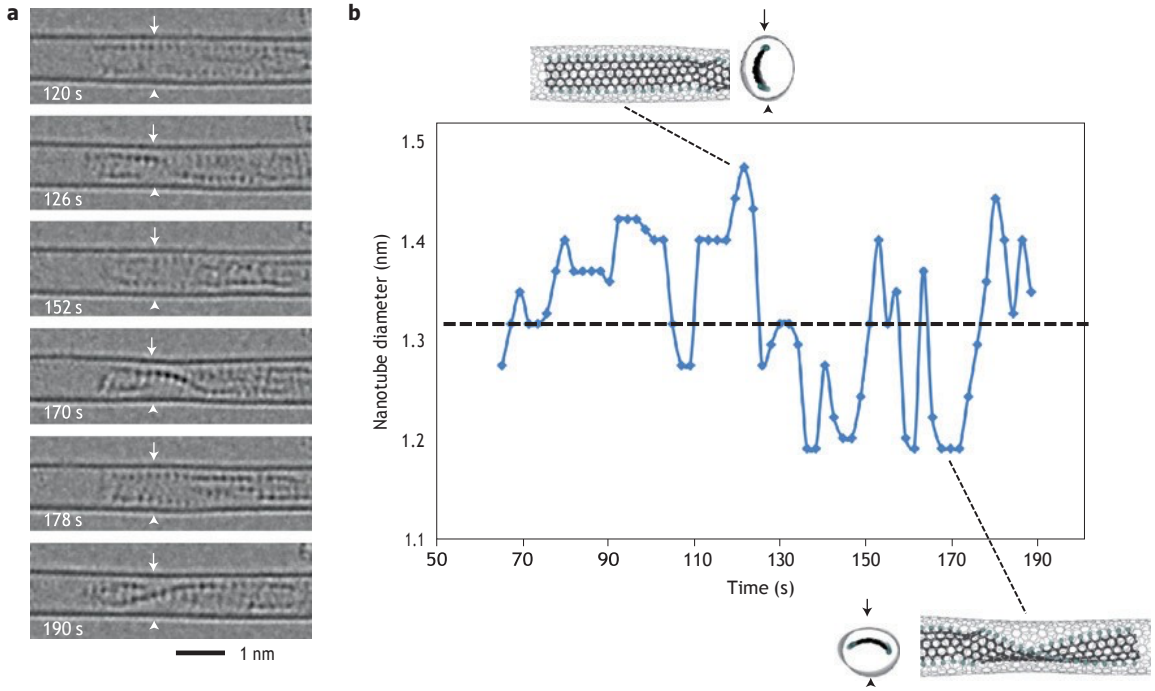

Figure 4 Dynamic behaviour of the nanoribbon inside the nanotube. a, A time series of images showing rotation of the S-GNR inside a carbon nanotube. The cross-section of the host-nanotube is elliptically distorted by the guest-nanoribbon: the nanotube is stretched within the plane of the S-GNR and contracted in the orthogonal plane. The projection of the nanotube diameter is measured for each image along the line designated by the two white arrows and (**b**) plotted as a function of time (dashed line indicates the nominal diameter of a cylindrical, undistorted (14, 5)-SWNT).

their elemental composition. We were not able to observe the actual mechanism of the nanoribbon formation from functionalized fullerenes or from TTF in direct space by AC-HRTEM, partly because the reactive intermediates move within the host-SWNT on a timescale much faster than the image capture rate (approximately 1 s). However, considering that the formation of S-GNR requires either irradiation with accelerated electrons or heating at very high temperature and is independent of the structure of the molecular precursors, the nanoribbon is likely to be formed from C_2 fragments and atomic sulphur generated from molecules broken down under these harsh conditions.

Sulphur atoms can bind to the edges of a zigzag nanoribbon using several different modes. AC-HRTEM imaging narrows down the possible options by revealing two important structural features of S-GNRs: the sulphurs atoms are positioned directly opposite each other across the nanoribbon width and are spaced equidistantly by $\sim 0.29 \pm 0.02$ nm along the nanoribbon edge (Fig. 3a). Considering that the S-GNR consists of three rows of hexagons, it is structurally related to peripentacene[25,26] and can be formally classified as a polythiaperipolycene. As such, the S-GNR possesses many resonance forms that would merge into a superposition (Fig. 3c). As a result, all S–S distances along the nanoribbon edge will be of the same length, corresponding to a bond order of less than one[27], which is consistent with the AC-HRTEM observations. Importantly, towards the end of the AC-HRTEM time series the equidistant separation between the sulphur atoms changesto an alternating pattern of long ($0.34 \sim 0.02$nm) and short(0.21 0.02 nm) S–S distances, which indicates a change in the bonding between the terminal atoms of the S-GNR induced by exposure to the e-beam (Fig. 3b). As the incident e-beam gradually removes valence electrons from the S-GNR (in chemical terms, the e-beam can be viewed as an oxidant) the pentagonal rings at the edges of the S-GNR turn into dithiolium cations (Fig. 3d), which are known to be very stable. In the presence of the cationic dithioliumgroups, the equidistant separation of S-atoms is no longer possible, as the resonance forms with S-atoms sitting in pairs within the dithiolium cation rings become predominant. The length of the S–S bond in dithiolium cations is known to be 0.21 nm (ref. 27), which is in agreement with the AC-HRTEM measurements.

The lengths of the nanoribbons observed in our experiments are in the range of 7–28 nm. However, it should be noted that the length measurements are limited by the field of view of HRTEM, because there is no fundamental reason why nanoribbons cannot be formed throughout the entire length of the host-nanotube, resulting in S-GNRs up to several micrometres long.

Owing to the fact that carbon atoms at the edges of the GNR have very different bonding characteristics to carbon atoms in the middle of the nanoribbon, zigzag GNRs are predicted to exhibit very unusual electron transport and magnetic properties[28–30]. Our spin-unrestricted density functional theory (DFT) calculations show that a S-GNR has a nonzero direct band gap of 0.5 eV, which issimilar in value to that of the H-terminated zigzag nanoribbons (H-GNR) (Fig. 3e,f). The electronic band gap in a zigzag GNRcan be controlled by an applied electric field[29,30], which opens up possibilities for the applications of GNRs in spintronics. Edge termination with sulphur atoms significantly lifts the energy of the Fermi level in S-GNR to 1.2 eV, as compared with 2.2 eVin H-GNR. Thus, a S-GNR is expected to possess strong electron donating properties, which may lead to a substantial electron transfer from the guest-nanoribbon to the host-nanotube (the typical Fermi level energy in the SWNT is 4.5 eV).

Our calculations show that the van der Waals width of the S-GNR exceeds the nominal diameter of the (14, 5) host-nanotube (1.32 nm), such that it would not be possible to insert a perfectly flat nanoribbon into a perfectly cylindrical nanotube. We have identified two mechanisms that allow for the nanoribbon to be accommodated within the nanotube. The first mechanism is the distortion of the SWNT cross-section into an elliptic shape (Fig. 4b). As the nanoribbon rotates inside the nanotube the nanotube seems to be expanding within the plane of the S-GNR and

contracting in the orthogonal direction (also see Supplementary Videos S1 and S3). The measured variation in the projected width of the host-nanotube is 0.25 nm, which corresponds to about 20% of the SWNT diameter and, therefore, imposes significant strain on the nanotube sidewall. The second mechanism is a spiral distortion of the nanoribbon itself (Fig. 4), which is a rather surprising result as nanoribbons synthesized outside the nanotubes are typically considered as flat, linear structures. Our time series AC-HRTEM imaging clearly demonstrates that the nanoribbon is a soft, flexible structure that can readily adopt a helical conformation, slightly resembling the shape of a party streamer. The spiral shape reduces the effective width of the S-GNR and potentially enables van der Waals interactions with the interior walls of the host-SWNT, which may additionally stabilize the S-GNR@SWNT structure. Notably, throughout the observation, the S-GNR remains mobile and rotates axially within the nanotube, thus indicating no chemical bonding between the nanoribbon and the nanotube container.

A previous theoretical study described non-planar configurations for narrow nanoribbons with unterminated edges (that is, containing highly unstable dangling bonds) predicting a 'saddle-shape chain' and a 'double helix' for these hypothetical GNRs (ref. 31). However, once both edges are terminated with H atoms,all the nanoribbons were predicted to adopt a strictly flat shape. In our case, the experimentally observed 'party streamer' heli- cal conformation of the GNR is qualitatively different to the predicted shapes[31] and is largely controlled by the confinement within the host-nanotube (similar to the atomic chains of iodine[32] or supramolecular chains of fullerenes[19] spontaneously forming helical arrangements in nanotubes of certain diameters). The helicaltwist of the nanoribbon can be a key parameter in determining the electromechanical properties of the GNRs, as their electronic band gaps are predicted to be critically dependent on the twist angle[33]. This could give rise to interesting piezoelectric effects at the nanoscale, as compression of the nanotube would result in changes in the electric properties of the GNR and vice versa.

This study outlines a new strategy for spontaneous self-assembly of GNRs with well-defined atomic structure from a mixture of atoms, using a SWNT as both the reaction vessel and template for nanoribbon growth, and presents the first example of GNR@SWNT—a new hybrid form of carbon nanomaterial.We identify the two key principles that lead to the formation of GNR: (1) 1D confinement at the nanoscale ensures propagation of the GNR in only one dimension, and (2) incorporation of heteroatoms into the predominantly carbon-based elemental feedstock leads to the termination of dangling bonds, stabilizing the structure. The surprising termination of nanoribbons with sulphur atoms may open avenues that have not been considered so far, even theoretically. The semiconducting properties of S-GNRs and the complex dynamic behaviour of the nanoribbon inside the nanotube (rotation and translation) observed in our study may pave the way for future applications of these materials in electronic and mechanical nanodevices. This new form of nanomaterial, where a 1D nanostructure is encapsulated within another 1D nanostructure, is likely to stimulate a new wave of experimental and theoretical studies.

Methods

Synthesis of the functionalized fullerene and its insertion into SWNTs. Details of the synthesis of *N*-methyl-2-(4-(lipoyloxy)benzyl)-[5,6]-$Sc_3N@C_{80}$ fulleropyrrolidine **1** are in the Supplementary Synthetic Methods. The structure of **1** was verified by spectroscopy before insertion into the nanotubes: MALDI-MS1447.14 *m/z* M^-. ^1H NMR 500 MHz, $CDCl_3$ CS_2 (1 6), 300 K δ_H 4.38 (*d*, *J* 9.7 Hz, 1H, CH_2 pyrrolidine), 3.76 (*s*, 1H, CH pyrrolidine), 3.15 (s, 3H, NCH_3), 3.08 (*d*, *J* 9.7 Hz, 1H, CH_2 pyrrolidine) ppm. HeteronuclearMultiple Quantum Correlation (HMQC) 500 MHz, $CDCl_3$ CS_2 (1 6), 300 K δ_C 85.0 (CH_2 pyrrolidine), 72.5 (CH pyrrolidine), 41.4 (NCH_3) ppm.

Compound **1** was inserted into nanotubes at room temperature from supersaturated chloroform solution (details are in the Supplementary Methods).

C_{60}/TTF@SWNT and TTF@SWNT preparation. Freshly annealed SWNTs (5 mg, NanoCarbLab, arc discharge) were added immediately to a mixture of tetrathiafulvalene (20 mg) and C_{60} (5 mg) at 150 °C under an argon atmosphere. The suspension was stirred for 3 h, allowed to cool, diluted with tetrahydrofuran (2 ml) and filtered onto a PTFE filtration membrane (pore size 0.5 μm). The material was then washed successively with tetrahydrofuran (10 ml) and methanol (10 ml) and dried in air. The process was repeated without the addition of C_{60} to yield a sample of TTF@SWNT.

Thermally activated formation of S-GNR. Samples of TTF@SWNT were sealed in three quartz tubes under a reduced pressure of argon (680 mbar). Each tube was heated at a different temperature; 250, 600 and 1,000 °C for 20 min, cooled to room temperature and opened. The products were mounted onto Si(100) supports and their Raman spectra were recorded at room temperature (HoribaJY LabRAM HR spectrometer, laser wavelength 532 nm). Only the sample heated at 1,000 °C indicated transformation of TTF into S-GNR (Supplementary Fig. S5) as Raman spectra of all samples heated at lower temperatures remained unchanged.

80 kV AC-HRTEM measurements. TEM investigation was performed on a Titan 80-300 (FEI, Netherlands) instrument equipped with an imaging-side aberration corrector. The instrument was operated at 80 kV accelerating voltage. To decrease the influence of the chromatic aberration, which is the limiting factor on resolutionat 80 kV, the extractor voltage of the electron gun was decreased to approximately 2,000 V, resulting in a better beam monochromaticity. The coefficient of the spherical aberration, C_S, of the objective lens was set to approximately 20 μm and a defocus of 13 nm was used (slightly below Scherzer defocus) to increase the contrast. The images were zero-loss filtered using a GIF Tridiem (Gatan, USA) andacquired by a Gatan Ultrascan 2K 2K CCD camera. The exposition time was 1 s, with approximately 2 s intervals between images for time series. Hardware binning 2 was used for a faster frame rate and to suppress the influence of the modulation transfer function (MTF) of the camera. Significant oversampling (0.023 nm/pix) was used to suppress further the influence of the MTF.

Details of image processing and image simulations are described in theSupplementary Methods and Figs S6 and S7.

Acknowledgements

This work was supported by by the DFG (German Research Foundation) and the Ministry of Science, Research and the Arts (MWK) of Baden-Württemberg in the frame of the SALVE (Sub Angstrom Low-Voltage Electron microscopy project) and by the DFG within the research project SFB 569 (U.K. and J.B.); the EPSRC (Career Acceleration Fellowship), NanoTP COST action and High Performance Computing (HPC) facility at the University of Nottingham (E.B.); the EPSRC, ESF and the Royal Society (A.N.K. and A.C.); the FP7 Marie Curie Fellowship (M.C.G-L.); and the Nottingham Nanoscience and Nanotechnology Centre (access to Raman spectrometer).

Author contributions

A.C. and J.B. carried out transmission electron microscopy experiments (Ulm University) and image analysis. E.B. and N.K. performed theoretical modelling. M.C.G-L. and T.W.C. synthesized materials. G.A.R. carried out Raman spectroscopy measurements. U.K. contributed to the development of the experimental methodology and the discussion of the results. A.N.K. proposed the chemical structure of nanoribbon and the pathway of its formation, and wrote the original manuscript. All authors discussed the results and commented on the manuscript.

Additional information

The authors declare no competing financial interests. Supplementary information accompanies this paper on www.nature.com/naturematerials. Reprints and permissions information is available online at http://www.nature.com/reprints. Correspondence and requests for materials should be addressed to A.N.K.

References

1. Berger, C. *et al*. Electronic confinement and coherence in patterned epitaxial graphene. *Science* **312,** 1191–1195 (2006).
2. Son, Y-W., Cohen, M. L. & Louie, S. G. Half-metallic graphene nanoribbons. *Nature* **444,** 347–349 (2006).
3. White, C. T. & Areshkin, D. A. Building blocks for integrated graphene circuits. *Nano Lett.* **7,** 825–830 (2007).
4. Yang, L., Cheol-Hwan, P., Son, Y-W, Cohen, M. L. & Louie, S. G. Quasiparticle energies and band gaps in graphene nanoribbons. *Phys. Rev. Lett.* **99,** 186801 (2007).
5. Wakabayashi, K. Electronic transport properties of nanographite ribbon junctions. *Phys. Rev. B* **64,** 125428 (2001).
6. Barone, V., Hod, O. & Scuseria, G. E. Electronic structure and stability of semiconducting graphene nanoribbons. *Nano Lett.* **6,** 2748–2754 (2006).
7. Datta, S. S., Strachan, D. R., Khamis, S. M. & Jonson, A. T. Crystallographic etching of few-layer graphene. *Nano Lett.* **8,** 1912–1915 (2008).
8. Li, X., Wang, X., Zhang, L., Lee, S. & Dai, H. Chemically derived, ultrasmooth graphene nanoribbon semiconductors. *Science* **319,** 1229–1232 (2008).
9. Kosynkin, D. V. *et al*. Longitudinal inzipping of carbon nanotubes to form graphene nanoribbons. *Nature* **458,** 872–875 (2009).
10. Jiao, L. Y., Zhang, L., Wang, X., Diankov, G. & Dai, H. Narrow graphene nanoribbons from carbon nanotubes. *Nature* **458,** 877–880 (2009).
11. Elias, A. L. *et al*. Longitudinal cutting of pure and doped carbon nanotubes to form graphitic nanoribbons using metal clusters as nanoscalpels. *Nano Lett.* **10,** 366–372 (2009).
12. Yang, X. Y. *et al*. Two-dimensional graphene nanoribbons. *J. Am. Chem. Soc.* **130,** 4216–4217 (2008).
13. Jiao, L., Wang, X., Diankov, G., Wang, H. & Dai, H. Facile synthesis of high-quality graphene nanoribbons. *Nature Nanotechnol.* **5,** 321–325 (2010).
14. Cai, J. *et al*. Atomically precise bottom-up fabrication of graphene nanoribbons. *Nature* **466,** 470–473 (2010).
15. Basiuk, V.A. & Basiuk, E.V. in *Chemistry of Carbon Nanotubes* Vol. 3, Ch. 5 (American Scientific Publishers, 2003).
16. Britz, D. A., Khlobystov, A. N., Porfyrakis, K., Ardavan, A. & Briggs, G. A. D. Chemical reactions inside single-walled carbon test-tubes. *Chem. Commun.* 37–39 (2005).
17. Bandow, S., Takizawa, M., Hirahara, K., Yudasaka, M. & Iijima, S. Raman scattering study of double-wall carbon nanotubes derived from the chains of fullerenes in single-wall carbon nanotubes. *Chem. Phys. Lett.* **337,** 48–54 (2001).
18. Britz, D. A. *et al*. Selective host–guest interaction of single-walled carbon nanotubes with functionalised fullerenes. *Chem. Commun.* 176–177 (2004).
19. Chamberlain, T. W. *et al*. Toward controlled spacing in one-dimensional molecular chains: Alkyl-chain-functionalized fullerenes in carbon nanotubes. *J. Am. Chem. Soc.* **129,** 8609–8614 (2007).
20. Gimenez-Lopez, M. C., Chuvilin, A., Kaiser, U. & Khlobystov, A. N. Functionalised endohedral fullerenes in single-walled carbon nanotubes. *Chem. Commun* **47,** 2116–2118 (2011).
21. Koshino, M. *et al*. Analysis of the reactivity and selectivity of fullerenes dimerization reactions at the atomic level. *Nature Chem.* **2,** 117–124 (2010).
22. Terrones, M. Electron microscopy: Visualizing fullerene chemistry. *Nature Chem.* **2,** 82–83 (2010).
23. Meyer, J. C. *et al*. Experimental analysis of charge redistribution due to chemical bonding by high-resolution transmission electron microscopy. *Nature Mater.* **10,** 209–215 (2011).
24. Williams, D. B. & Carter, C. B. *Transmission Electron Microscopy: A Textbook for Materials Science* (Plenum, 1996).
25. Goodings, E. P., Mitchard, D. A. & Owen, G. Synthesis, structure, and electrical properties of naphthacene, pentacene, and hexacene sulphides. *J. Chem. Soc. Perkin Trans.* 1310–1314 (1972).
26. Briseno, A. L. *et al*. Hexathiapentacene: Structure, molecular packing, and thin-film transistors. *J. Am. Chem. Soc.* **128,** 15576–15577 (2006).
27. Klingsberg, E. Thiothiophethene no-bond resonance compounds. *Quart. Rev.* **23,** 537–551 (1969).
28. Son, Y-W., Cohen, M. L. & Louie, S. G. Energy gaps in graphene nanoribbon. *Phys. Rev. Lett.* **97,** 216803 (2006).
29. Rudberg, E., Salek, P. & Luo, Y. Nonlocal exchange interaction removes half-metallicity in graphene nanoribbons. *Nano Lett.* **7,** 2211–2213 (2007).
30. Hod, O., Barone, V., Peralta, J. E. & Scuseria, G. E. Enhanced half-metallicity in edge-oxidised zigzag graphene nanoribbons. *Nano Lett.* **7,** 2295–2299 (2007).
31. Bets, K. V. & Yakobson, B. I. Spontaneous twist and intrinsic instabilities of pristine graphene nanoribbons. *Nano Res.* **2,** 161–166 (2009).
32. Fan, X. *et al*. Atomic arrangement of iodine atoms inside single-walled carbon nanotube. *Phys. Rev. Lett.* **84,** 4621–4624 (2000).
33. Gunlycke, D., Li, J., Mintmire, J. W. & White, C. T. Edges bring new dimension to grapheme nanoribbons. *Nano Lett.* **10,** 3638–3642 (2010).

Supporting Information file

Computational Methods

Comparative thermodynamic stability of carbon nanostructures

Upon unfolding a single-walled carbon nanotube (SWNT), the newly formed graphene nanoribbon (GNR) experiences the loss of chemical bonds at the edges, which causes the GNR to be less thermodynamically stable than the corresponding SWNT. In this work, we compare a GNR of similar width to the diameter, not circumference, of a SWNT (i.e. a much narrower GNR than those obtained by simply unfolding the SWNT). The wider GNRs become more stable, through the lowering of cohesive energy, thus approaching the limit of graphene. Passivation of the bare edges with termination groups further stabilises the structure.

To quantify the above conclusions it is necessary to evaluate the relative stability of GNRs both with and without edge passivation. As these GNRs may have different chemical compositions, the straightforward computation of the cohesive energy per atom does not provide a suitable way to compare their relative stability. We adopt the approach widely used in binary phase thermodynamics to account for chemical composition and define a molar (per atom) Gibbs free energy of formation δG for a GNR as

$$\delta G = -E - x_{term}\ _{term} - (1 - x_{term})\ _{C},$$

where E is the cohesive energy (per atom) of the nanostructure, x_{term} is the molar fraction of terminus atoms, and $_{term}$ and $_{C}$ are the chemical potentials of the constituents. We chose $_{H}$ to be the binding energy (per atom) of the H_2 molecule, $_{S}$ - the cohesive energy (per atom) of the most stable isomer of sulphur S_8, and $_{C}$ - the cohesive energy (per atom) of graphite. This definition allows us a direct comparison of the relative stabilities between terminated and non-terminated GNRs with different chemical compositions.

Table S1 summarises the data for cohesive energies and Gibbs free energies of formation of guest nanostructures with different chemical compositions. In this work, the μ_C value is taken to be -7.37 eV, that ofthe experimental cohesive energy of graphite,[S1] μ_H=-2.37 eV/atom,[S2,S3] and μ_S=-1.32 eV/atom.[S4] In all 'pure carbon' cases x_{term}=0, and for nanoribbons terminated with hydrogen (H-GNR) and sulphur (S-GNR) the molar fraction of terminus atoms is x_{term}=0.2. The calculations of the cohesive energies E have been obtained for the optimized structures of infinite SWNTs and GNRs using CASTEP quantum chemistry code,[S5] which employs the density functional theory plane-wave pseudopotential method. A plane wave basis set with the energy cut-off of 390 eV has been used. For the exchange correlation term the Generalised Gradient Approximation (GGA) has been used in the form of the PBE functional.[S6] "On-the-fly" pseudopotentials generator has been used as implemented in CASTEP. Parameter d in Table S1 is the diameter in the case of SWNTs and the width in case of GNRs.

Supplementary Table 1. Gibbs free energies of formation and cohesive energies of guest nanostructures encapsulated in SWNT.

nanostructure	graphite	(13,0) SWNT	(9,0) SWNT	non-terminated GNR	H-GNR	S-GNR
d, Å	-	10.3	7.2	7.1	9.3	10.7
δG, eV/atom	0	0.71	0.79	1.23	0.57	0.58
E, eV/atom	7.37	6.66	6.58	6.14	5.80	5.58

It can be seen from Table S1 that SWNTs are less stable than the terminated GNRs. Both the slightly narrower H-GNR with the width of 9.3 Å and the S-GNR with the width of 10.7 Å have similar thermodynamic stability, and the value of the Gibbs free energy of formation (δG) is less than that ofSWNTs. If terminus atoms are stripped off, the bare (non-terminated) GNR has a significantly higher δG (andis therefore less stable) than that of SWNTs.

Therefore, the stability of the guest system formed within the interior of a SWNT increases from the non-terminated GNRs to SWNTs of small diameter, and from SWNTs to the terminated nanoribbons. In the absence of heteroatoms inside the nanotube fullerenes will evolve into the guest SWNT, while if Sulphur or reactive Hydrogen atoms are present a terminated GNR will form.

Electronic properties of graphene nanoribbons

The calculations of the electronic properties are performed using the CASTEP code.[S5] To describe exchange and correlation interactions the spin-polarized generalised gradient approximation (GGA) is used in the form of the Perdew-Burke-Ernzerhof (PBE) functional.[S6] Ultrasoft pseudopotentials are generated using the "on-the-fly" formalism available in CASTEP. A plane wave cut-off energy is set to 500 eV, and the convergence threshold for energy is 10^{-6} eV. A *k*-point sampling of 45 *k* points that are uniformly positioned along the 1D Brillouin zone of the nanoribbon is employed. The geometry of the nanoribbons is fully relaxed until the force on each of the atom is less than 0.05 eV/Å.

Synthetic Methods

Synthesis and characterisation of *N*-methyl-2-(4-(liponyloxy)benzyl)-[5,6]-$Sc_3N@C_{80}$ fulleropyrrolidine.

All other reagents and solvents were purchased from Aldrich and were used without further purification. ^1H and ^{13}C NMR spectra were obtained on a Bruker AV(III)500 spectrometer. Coupling constants (*J*) are denoted in Hz, and chemical shifts (δ), in ppm. Mass spectrometry was carried out on a Bruker Ultraflex III MALDI-TOF spectrometer using DCTB as matrix (355 nm).

A mixture of 0.8 mg of $Sc_3N@C_{80}$ (Luna Innovations; 7.6 10^{-4} mmol), 1.1 mg of sarcosine (0.013 mmol) and 13.0 mg of 4-(liponyloxy)benzaldehyde (0.04 mmol) was heated and stirred at 110 ºC in 15 mL of dry toluene for 270 min. The crude product was purified by column chromatography (silica gel/toluene; R_f = 0.13) affording compound **1** in a 34 % yield. MALDI-MS 1447.14 *m/z* $[M]^-$. ^1H NMR {500 MHz, $CDCl_3$:CS_2 (1:6), 300 K} δ_H 4.38 (d, J = 9.7 Hz, 1H, $-CH_2$ pyrrolidine), 3.76 (s, 1H, –CH pyrrolidine), 3.15 (s, 3H, $-NCH_3$), 3.08 (d, J = 9.7 Hz, 1H, $-CH_2$ pyrrolidine) ppm. Heteronuclear Multiple Quantum Correlation

(HMQC) {500 MHz, $CDCl_3$:CS_2 (1:6), 300 K} δ_C 85.0 (–CH_2 pyrrolidine), 72.5 (–CH pyrrolidine), 41.4 (–NCH_3) ppm.
MALDI-TOF mass spectrum of **1** (inset: isotopic distribution pattern confirming the composition of monoadduct **1**). Heteronuclear Multiple Quantum Correlation (HMQC) of **1**{500 MHz, $CDCl_3$:CS_2 (1:6), 300 K} δ_C 85.0 (–CH_2 pyrrolidine), 72.5 (–CH pyrrolidine), 41.4 (–NCH_3) ppm.

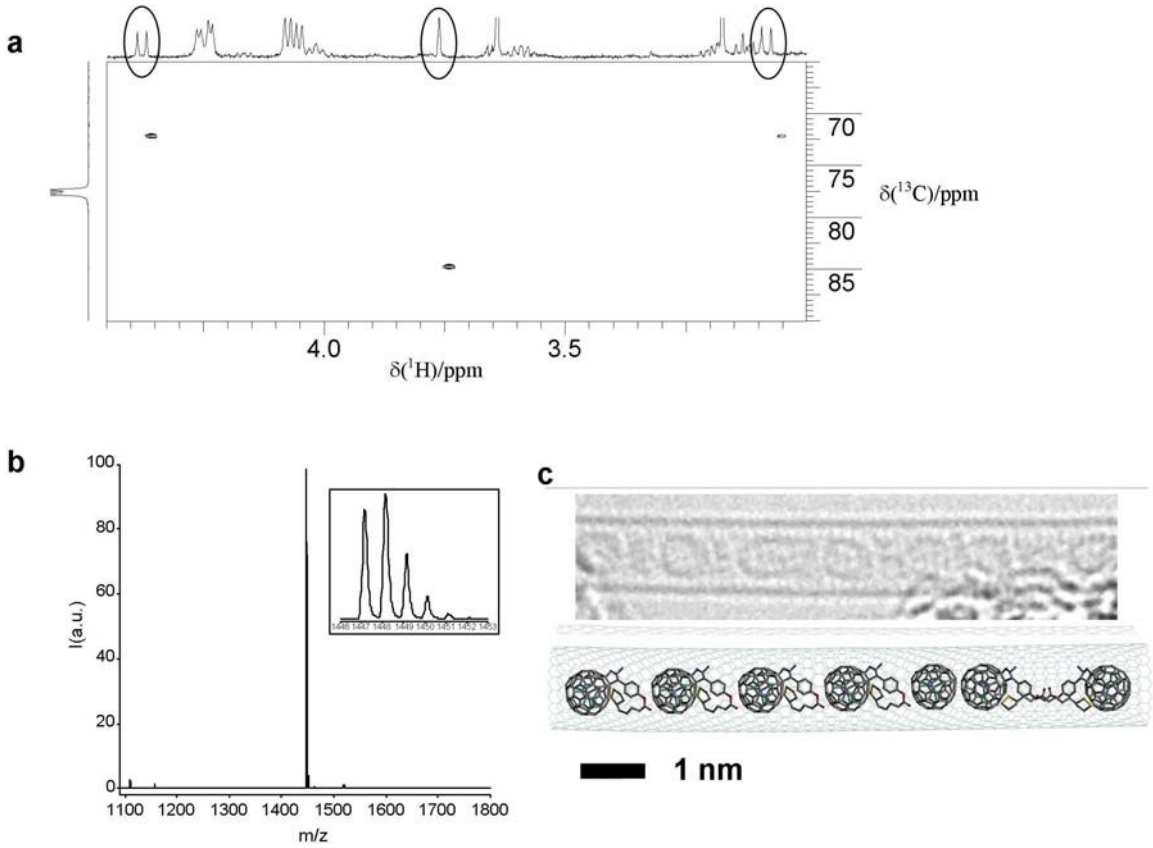

Supplementary Figure 1. (a) NMR and (b) mass spectrometry data for compound **1**. (c) AC-HRTEM image and structural diagram of a chanin of **1** molecules within SWNT.

Insertion of functionalised fullerene molecules into carbon nanotubes

5 mg of SWNT (*NanoCarbLab*, arc discharge) heated in air at 520 ºC for 38 min were added immediately after heating to a solution of compound **1** (50 μg) in 0.05 ml of chloroform at room temperature. The solvent was evaporated, an additional amount of chloroform was added (0.05 ml) and the resultant mixture was stirred vigorously until the solvent evaporated again. This procedure was repeated three times. The resultant black powder was dispersed in 20 mL of chloroform under ultrasonic agitation; the suspension was filtered onto a PTFE filtration membrane (pore size 0.5 μm), washed with an additional 10 mL portion of chloroform and dried in air.

Formation of nanoribbons from tetrathiafulvalene, and tetrathiafulvalene/C_{60} mixtures in SWNT

The molecular precursors from which GNR can be generated within SWNT are not limited to functionalised fullerenes. A mixture of pristine C_{60} and tetrathiafulvalene (TTF, $C_6H_4S_4$) was inserted into

SWNT using a molten blend of the two molecules at elevated temperatures. Both continuous GNR@SWNT structures (black arrow) and discrete C_{60} molecules beginning to merge into GNR (white arrows) are observed within the nanotube at the early stages of imaging (Figure 2). The fact that nanoribbons are formed from such precursors confirms that the presence of a sulphur containing species within the nanotube is essential, as no evidence of any nanoribbon formation has ever been reported for pure C_{60}@SWNT systems due to the preferential formation of internal nanotubes.

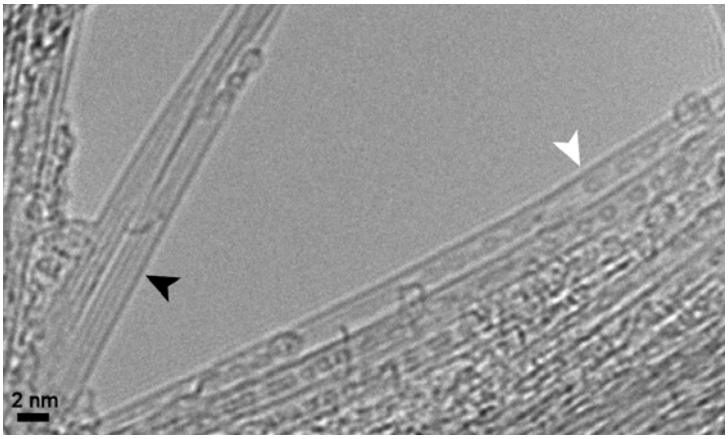

Supplementary Figure 2. HRTEM large field of view image of C_{60}/TTF@SWNT depicting initial stages of S-GNR@SWNT structures formation under the electron beam. Fullerene molecules beginning to react within the nanotube and fully formed S-GNRs are marked by a white and black arrow respectively.

Further investigation demonstrated that it is actually possible to use TTF as the source of both carbon and sulphur to generate GNRs. HRTEM analysis of tetrathiafulvalene encapsulated inside SWNT in the absence of fullerene shows that nanoribbons can be generated by the e-bream (Figure 3a). Similarly to the nanoribbons derived from functionalised fullerenes, these GNRs are observed to rotate within the nanotube cavity under irradiation by the electron beam (Supplementary video file, *TTF_nanoribbon.avi*).

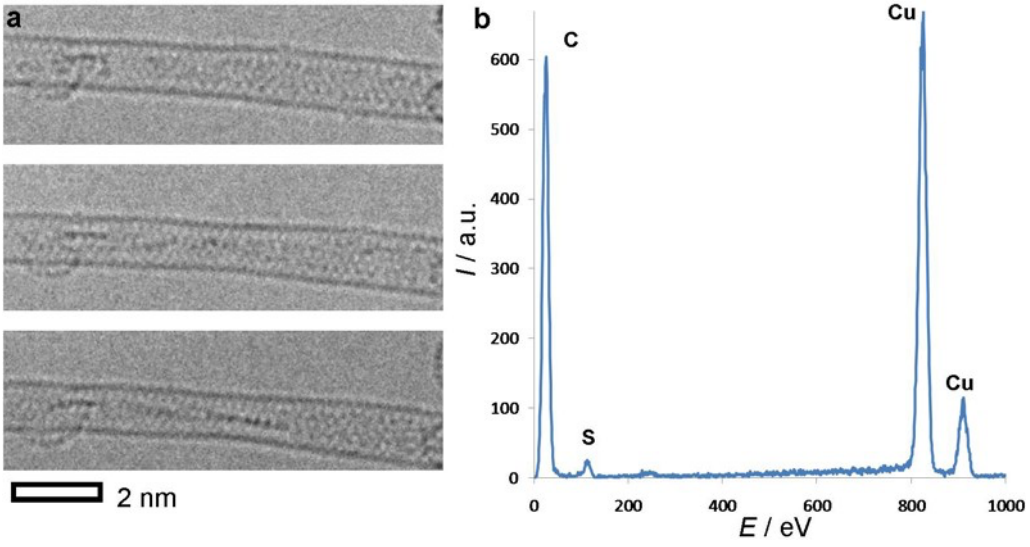

Supplementary Figure 3. a) AC-HRTEM image series showing S-GNR@SWNT structures formed from tetrathiafulvalene rotating over time; b) EDX spectrum of a small bundle of S-GNR@SWNT confirming the presence of sulphur at the edges of the nanoribbon (copper peaks are due to the specimen holder).

Energy dispersive X-ray (EDX) spectroscopy of a small bundle of S-GNR@SWNT confirms the identity of the terminating atoms (Figure 3b). Although sulphur is present only in a very small quantity in the S-GNR@SWNT structure, the EDX peak of sulphur can be observed clearly.

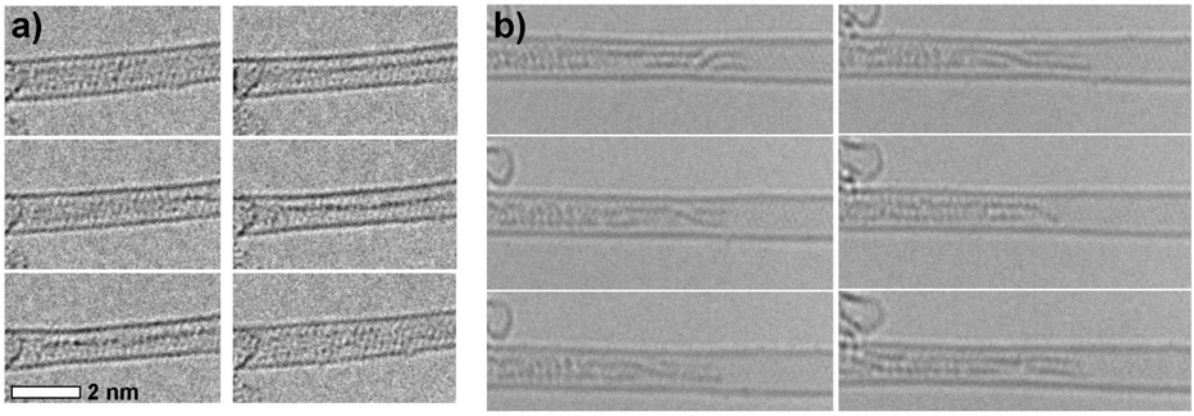

Supplementary Figure 4. Time series of AC-HRTEM images showing different examples of S-GNR@SWNT structures formed from carbon- and sulphur-containing molecules.

Although the Raman spectrum of TTF@SWNT is dominated by bands of the SWNT, two bands of TTF were consistently observed at ~1420 cm^{-1} and 490 cm^{-1}, corresponding to C=C stretch and pentagonal ring bend respectively[S13] (Figure 5 and inset, peaks labelled by a star). Transformation of TTF into nanoribbons can be thermally activated at 1000 ºC. High temperature is required to break down TTFmolecules and re-assemble the atoms of C and S into S-GNR, since no transformation takes place (*i.e.* Ramanspectrum is unchanged with bands of TTF still present) at 250 ºC and 600 ºC. However, after 20 min of heating at 1000 ºC, all peaks of TTF disappear and a new peak emerges at ~1200 cm^{-1}, which is attributed to C=S bonds at the edge of the S-GNR (Figure 5, inset: peak labelled by two stars). All vibrations of carbon- carbon bonds of the nanoribbon are obscured by the peaks of SWNT container.

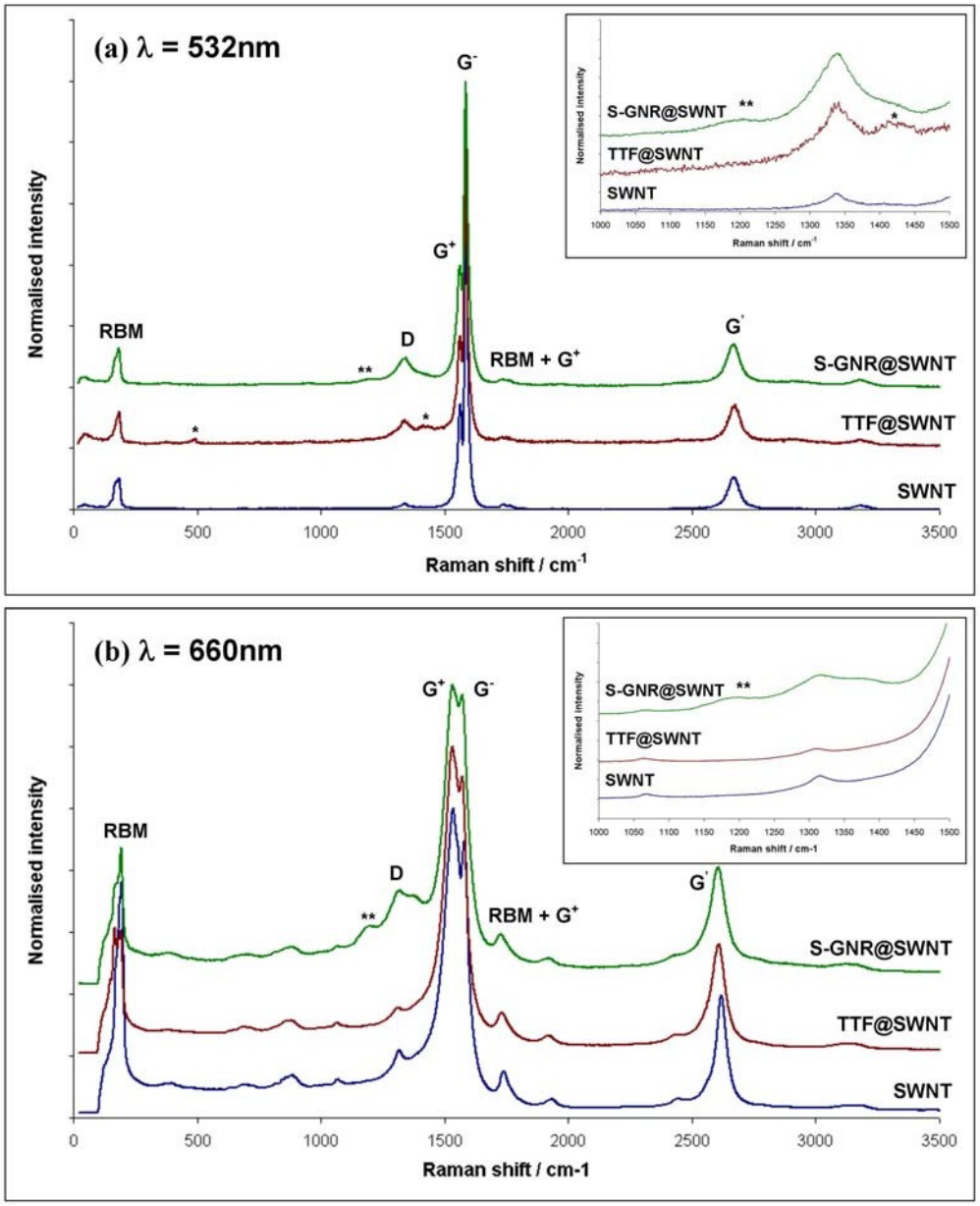

Supplementary Figure 5. Raman spectra of TTF@SWNT (middle trace), S-GNR@SWNT formed at 1000 °C (top trace) and a control sample of empty nanotubes (bottom trace). Inset: expanded area from 1000 to 1500 cm^{-1}. To guide the eye, the vibrational bands of TTF and S-GNR are marked by single and double stars respectively. The two sets of spectra were recorded at different laser wavelengths λ = 532 nm (top set) and λ = 660 nm (bottom set).

Electron Microscopy Methods

Image Filtration

In order to reveal the structure of GNR images of front and back walls of the nanotube were removed by Fourier filtering. To minimise the statistical noise the images were treated by Gaussian blur filter. Fig 6 represents original and processed images along with their FFTs.

Fourier filtering is a well established image processing technique,[S7-S9] which is particularly useful for the removal of the periodic background lattice of carbon nanostructures.[S10] The method utilises the fact that in frequency domain signals from periodic objects are highly localised and thus can be easily eliminated without

detrimental effects on the rest of the image. Below we provide unprocessed images and describe in detail all processing steps. The same procedure applied to simulated images clearly improved the visibility of nanoribbons without introducing any artefacts.

The main reason why the atomic structure of the ribbon cannot always be clearly seen is the translational and rotational motion of GNR. This motion accounts for the main differences between experimental and simulated images. For the later, only thermal vibrations of individual atoms about their equilibrium positions were considered (Debye-Waller factor). Mathematical description of the nanoribbon's motion is too uncertain at this stage due to many stochastic factors, and thus the motion could not be accounted for in the image simulation.

Although the GNR was observed to move continuously, on rare occasions it remained still thus allowing atomic resolution of the carbon hexagons, as shown in Fig2c and Fig4a. The observation of the graphitic structure of GNR in these images enables unambiguous determination of the nanoribbon structure.

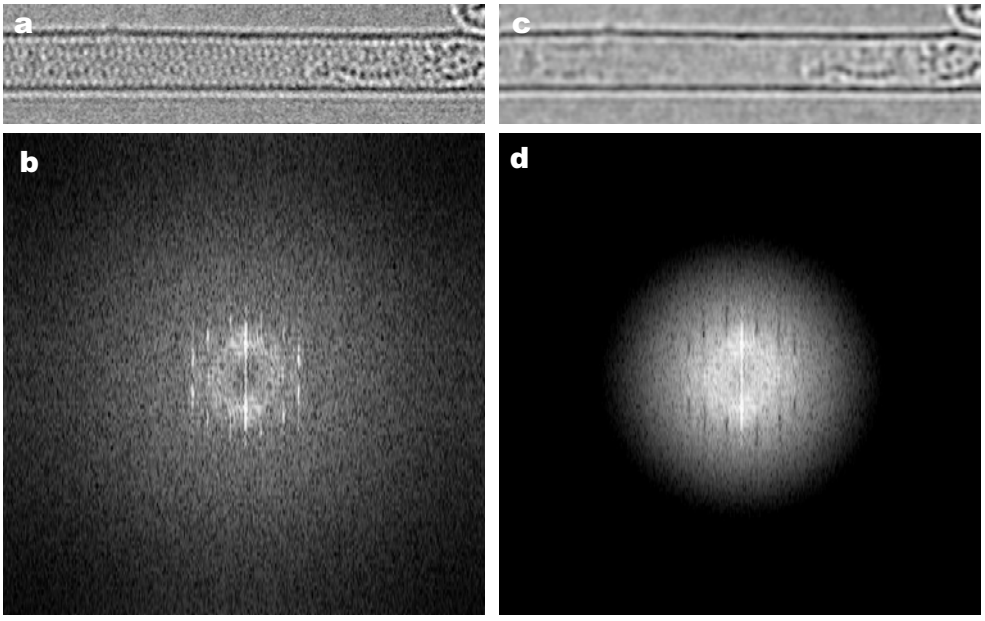

Supplementary Figure 6. (a) Original image as acquired within time series, (b) FFT of (a), (c) processed image as presented in the paper, (d) FFT of (c).

SWNT index determination

Indexes of SWNT presented in the paper and Supplementary video 1 were determined from the FFT of the images of the empty part of the nanotube, as shown in Fig. 7. The chiral indices are uniquly determined as (14, 5) following an established procedure.[S11] This nanotube was used further for image simulations.

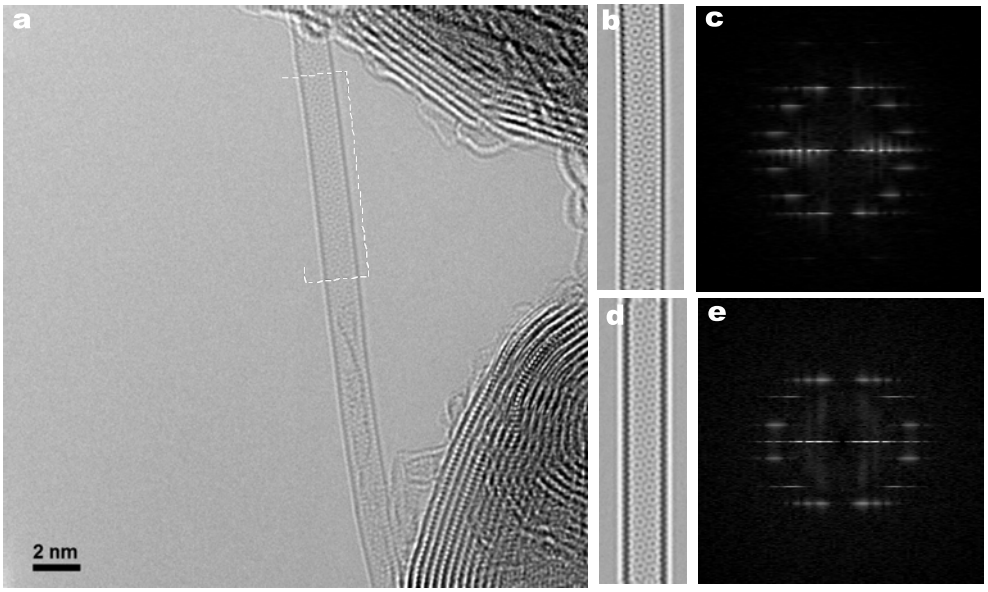

Supplementary Figure 7. (a) Overview image of the nanotube containing GNR with a rectangle marking the region used for analysis, (b) multiple frames average of the image of the marked area, (c) FFT of the experimental image of a (14, 5) SWNT, (d) simulated image of a (14, 5) SWNT and (e) FFT of the simulated image of a (14, 5) SWNT.

Image simulations

TEM image simulations were performed using a custom-made programme (MUSLI code).[S12] Coherent aberrations corresponding to those in the experimental images were used. Parameters for the dumpingenvelope were as follows: focal distance 1.5 mm (tabulated value for Titan 80-300), coefficient of chromatic aberration 1.4 mm (measured experimentally), energy spread of electron source 0.2 eV (measured experimentally), stability of high tension 10^{-6} (tabulated value for Titan 80-300), stability of objective lens current $3 \cdot 10^{-7}$ (fitted by simulations), convergence semi-angle 0.5 mrad (this parameter does not measurably influence aberration corrected imaging). The sampling rate was 0.015 nm/pixel. Images were calculated at theelectron dose of 10^6 e^-/nm^2 and further processed using the same routine as for experimental images.

Atomistic models for image simulations were optimized using MM+ empirical potentials including van der Waals interactions.

References:

S1. Kittel, C. *Introduction to Solid State Physics* 5th edn (New York: Wiley) 74 (1976)
S2. Kolos, W. & Wolniewicz, L. Accurate Adiabatic Treatment of the Ground State of the HydrogenMolecule. *J. Chem. Phys*. **41**, 3663-3673 (1964)
S3. Kolos, W. & Wolniewicz, L. Improved theoretical ground-state energy of the hydrogen molecule. *J. Chem. Phys*. **49**, 404-410 (1968)
S4. Jones, R.O. & Ballone, P. Density functional and Monte Carlo studies of sulfur. I. Structure and bonding in S_n rings and chains (n = 2-18). *J. Chem. Phys*. **118**, 9257-9265 (2003)
S5. Payne, M.C., Teter, M.P., Allan, D.C., Arias, T.A. & Joannopoulos, J.D. Iterative minimization techniques for ab initio total-energy calculations: molecular dynamics and conjugate gradients. *Rev. Mod. Phys.* **64**, 1045-1097 (1992)
S6. Perdew, J.P., Kieron, B & Ernzerhof, M. Generalized gradient approximation made simple. *Phys. Rev. Lett.* **77**, 3865-3868 (1996)
S7. Russ, J. C. The image processing handbook, 4th ed., *CRC Press*, Boca Raton. 732 p., (2002)
S8. Li, S.-Y. & Ye, H.-Q. Digital enhancement of the surface contrast in a conventional HREM image, *Ultramicroscopy* **74**, 27-33 (1998)
S9. Scanning Transmission Electron Microscopy, Imaging and Analysis, Eds. Pennycook, S.J. & Nellist, P.D. *Springer* (2011)

S10. Chuvilin, A., Meyer, J.C., Algara-Siller, G. & Kaiser, U. From graphene constrictions to single carbon chains, *New J. Phys.* **11**, 083019 (2009)
S11. Qin L. C., Determination of the chiral indices (n,m) of carbon nanotubes by electron diffraction, *Phys. Chem. Chem. Phys.* **9**, 31–48 (2007)
S12. Chuvilin, A. & Kaiser, U. On the peculiarities of CBED pattern formation revealed by multislice simulation. *Ultramicroscopy* **104**, 73-82 (2005)
S13. Berlinsky, A.J., Hoyano, Y. & Weiler, L. Raman spectra of tetrathiofulvalene (TTF). *Chem. Phys. Lett.* **45**, 419-421 (1977)